

One-Dimensional Photonic Crystal for Surface Mode Polarization Control

Erika Moggi, Giovanni Pellegrini, Jorge Gil-Rostra, Francisco Yubero, Giuseppina Simone, Stefan Fossati, Jakub Dostálek, Rebeca Martínez Vázquez, Roberto Osellame, Michele Celebrano, Marco Finazzi, and Paolo Biagioni*

Bloch surface waves sustained by truncated 1D photonic crystals (1DPCs) are well known tools for surface-enhanced spectroscopy. They provide strongly confined fields with uniform distribution over a large surface area, a characteristic exploited in standard refractometric sensing. However, their application to polarization-sensitive investigations is not straightforward because the transverse electric (TE) and magnetic (TM) surface modes possess distinct dispersion relations, therefore their relative phase is not conserved along propagation and the polarization state of any wave obtained by combining these modes is ill-defined. In this work, a novel design of a 1DPC is realized in which the TE and TM modes exhibit the same phase velocity over a broad-band spectral range and thus their dispersion relations overlap. The capability to simultaneously excite TE and TM modes with a well-defined phase relation allows the generation of surface waves with a controlled polarization state. This paves the way to polarization-resolved surface-enhanced analysis, including, for example, linear and circular dichroism spectroscopy of grafted molecular layers at the photonic crystal surface.

materials with different refractive indices, that is, a multilayer film where the material is homogeneous in the plane of the surface while periodic in the direction perpendicular to it. The refractive index contrast between the constitutive layers produces a photonic band gap where no purely real wave vector is allowed. Instead, for frequencies within the band gap the mode wave vector is complex, resulting in a wave that exponentially vanishes into the crystal. Thanks to their high sensitivity to the local refractive index, BSWs can be exploited as a sensing tool for analytes located at the surface of truncated photonic crystals.^[1–5] Moreover, the design of 1DPCs offers the possibility to tune the resonance frequencies of the modes by selecting the materials (i.e., the refractive index) and thicknesses of the layers. A further step in surface-enhanced spectroscopy using BSWs would be the control


1. Introduction

Bloch Surface Waves (BSWs) are supported by semi-infinite 1D photonic crystals (1DPCs). The eigenmodes can be described as a series of the transverse electric (TE) and transverse magnetic (TM) ones.^[1] The simplest possible 1DPC consists of a periodic alternance of layers of two (ideally non-absorbing)

over their polarization, which can be attained by engineering the overlap between the dispersion relations of the TE and TM modes. For example, the surface-enhanced study of oriented molecules anchored to the 1DPC surface could be approached via differential TE-TM reflectivity measurements, as customarily done in standard attenuated total internal reflection spectroscopy.^[6,7] More specifically, the superposition of the TE and

E. Moggi, F. Yubero, G. Simone, M. Celebrano, M. Finazzi, P. Biagioni
Dipartimento di Fisica
Politecnico di Milano
Piazza Leonardo Da Vinci 32, Milano 20133, Italy
E-mail: paolo.biagioni@polimi.it

G. Pellegrini
Dipartimento di Fisica
Università degli studi di Pavia
Via Bassi 6, Pavia 27100, Italy

 The ORCID identification number(s) for the author(s) of this article can be found under <https://doi.org/10.1002/adom.202200759>.

© 2022 The Authors. Advanced Optical Materials published by Wiley-VCH GmbH. This is an open access article under the terms of the Creative Commons Attribution License, which permits use, distribution and reproduction in any medium, provided the original work is properly cited.

DOI: 10.1002/adom.202200759

J. Gil-Rostra, F. Yubero
Instituto de Ciencia de Materiales de Sevilla
CSIC-Universidad de Sevilla
Sevilla 41092, Spain

G. Simone
School of Mechanical Engineering
Northwestern Polytechnical University
Xi'an, Shaanxi 710081, P. R. China

S. Fossati, J. Dostálek
Biosensor Technologies
AIT-Austrian Institute of Technology GmbH
Tulln an der Donau 3494, Austria

J. Dostálek
FZU-Institute of Physics
Czech Academy of Sciences
Prague 18221, Czech Republic

R. Martínez Vázquez, R. Osellame
Istituto di Fotonica e Nanotecnologie (IFN)-CNR
Piazza Leonardo da Vinci 32, Milano 20133, Italy

TM modes enables linear and circular dichroism (CD) spectroscopy. The former measures the difference in the molecular absorption of light polarized linearly along two perpendicular directions,^[8] providing information about the conformation and orientation of structures within molecules.^[9,10] Instead, CD measures the differential absorption of left and right circularly polarized light, which constitutes the most common approach for the investigation of chiral molecules. CD is gaining more and more importance due to wide applications in chemistry, biology, medicine, and pharmacology.^[11,12] In general, CD signals are very weak if compared to those of standard absorption spectroscopy, which makes the analysis of small amounts of chiral analytes extremely challenging. Recently, novel “superchiral” approaches have been introduced to enhance the CD signal by engineering the optical chirality of the electromagnetic field with the use of nanostructured systems.^[13,14] The term “superchiral” originally referred to electromagnetic field configurations that allow one to detect larger differential signals from chiral molecules with respect to plane wave illumination but nowadays it is commonly used to describe electromagnetic fields exhibiting optical chirality larger than that of circularly-polarized plane waves. Many efforts have been devoted to exploit this property with approaches based on both metallic and dielectric nanostructures that generate hotspots of enhanced optical chirality.^[15–34] In this framework, we recently introduced a novel design of the 1DPC^[3] that allows for the generation of “superchiral” surface waves. This allows for the enhancement of the CD signal by more than two orders of magnitude (possibly down to the monolayer sensitivity), with a broadband spectral range and uniform surface fields not limited to confined hot spots. In particular, the design of a 1DPC terminated with an additional anisotropic surface multilayer allows one to engineer the dispersion relations of the TE and TM surface modes and superpose them coherently to generate specific polarization configurations based on the relative phase difference between the two modes. In this work, we realize a 1DPC platform designed specifically to reduce the total number of layers compared to the original design^[3] while still keeping the same polarization performance and we experimentally demonstrate the superposition of the dispersion relations of the TE and TM modes, paving the way to the employment of such a platform for surface-enhanced polarization-sensitive

spectroscopy in the visible-UV range and more generally to the implementation of polarization-resolved surface-enhanced techniques.

2. Design and Fabrication of the Optofluidic Platform

2.1. Photonic Design

We conceptually rely upon the original truncated 1DPC design,^[3] where the photonic platform was terminated with an anisotropic truncation realized through an additional, shorter period, multilayer on top of the original 1DPC, for a total of 13 layers overall. Here we demonstrate that such a design can be considerably simplified by substituting the whole termination multilayer with just a single high refractive index inclusion inside the last low-index layer of the 1DPC. This configuration still allows for the tuning of the TE and TM dispersion relations by changing the thickness and position of the high index inclusion, while altogether avoiding the complexity introduced by an additional short-period multilayer. Moreover, this design further simplifies the fabrication of the 1DPC by avoiding the use of extremely thin layers as those proposed in ref. [3]. A realization of the simplified design is illustrated in **Figure 1** (panel a), together with an experimental observation of the cross-section by scanning electron microscopy (SEM, panel b) of the multilayer grown by reactive magnetron sputtering, as discussed later in the manuscript.

The multilayer consists of alternating high (n_H) and low (n_L) refractive index materials, for a total of only 7 layers (2 periods of the 1DPC plus 3 layers for the termination), whose thickness has been optimized to maximize the overlap of the TE and TM modes in an aqueous-based environment. The adopted materials are alternating Ta_2O_5 (n_H) and SiO_2 (n_L) placed on a BK7 substrate. The optical constants of the chosen materials are retrieved from the literature^[35,36] with the addition of a small offset $\Delta k = 0.001$ to the imaginary part of the refractive index of Ta_2O_5 to better reproduce the experimental observations. We simulate the system by using a Fresnel reflectivity model with the transfer matrix method, in order to capture the momentum matching with Kretschmann configuration.^[37] The thicknesses employed for the simulations are obtained by the concurrent fitting of the experimental TE and TM reflectivities at a wavelength of 405 nm, which delivers thickness values with deviations of up to 10 nm for the thick layers and of about 3 nm for the thin high-index inclusion. Such thickness variations from the nominal design are typically expected and can be ascribed to both the effect of actual thickness deviations and of small uncertainties in the refractive index of the materials. The resulting dispersion relations are reported in the simulated reflectivity maps of **Figure 2** for TE and TM illumination (panels a and b, respectively), together with representative angular plots at specific wavelengths (panels c–e), confirming the good partial overlap of the two modes. We also simulated, as demonstrated in **Figure S1**, Supporting Information, the TE and TM band structures of the infinite 1DPC, together with the dispersion relations of the respective surface modes.

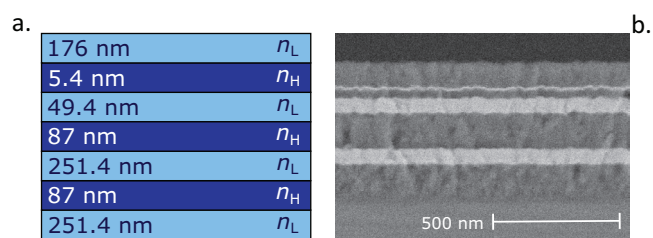


Figure 1. a) Schematic representation of the 1DPC design. Layers with different refractive indices are represented with different colors. The nominal reported thicknesses of each layer in the fabricated sample are extracted from the numerical simulations at a wavelength of 405 nm (see **Figure 2**), after the concurrent fitting of both TE and TM reflectivities. b) Cross section SEM image of the truncated 1DPC deposited on a polished silicon wafer. Brightness contrast between layers is due to the different atomic weights of the Ta_2O_5 (light layers) and SiO_2 layers (dark layers).

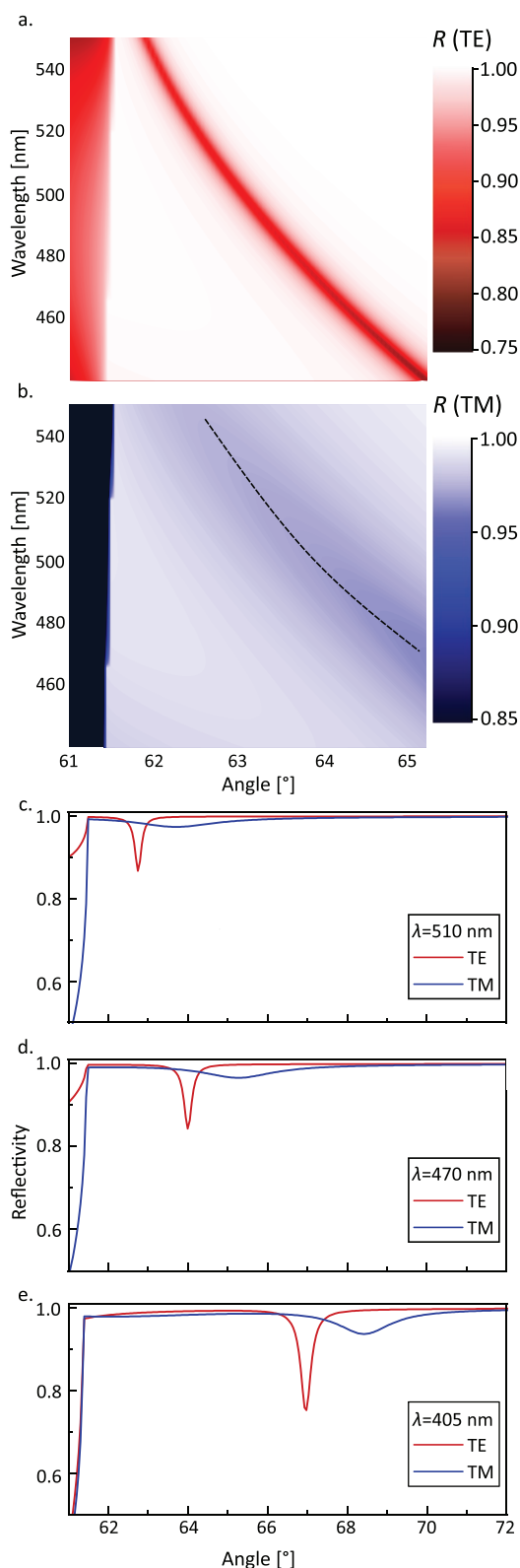


Figure 2. Numerically simulated reflectivity (R) maps for a) TE and b) TM polarization when the surface is contacted with water. The dispersive TE and TM modes are visible as dips in the reflectivity maps as illustrated by the angular reflectivity plots for a wavelength λ equal to c) 510, d) 470, and e) 405 nm.

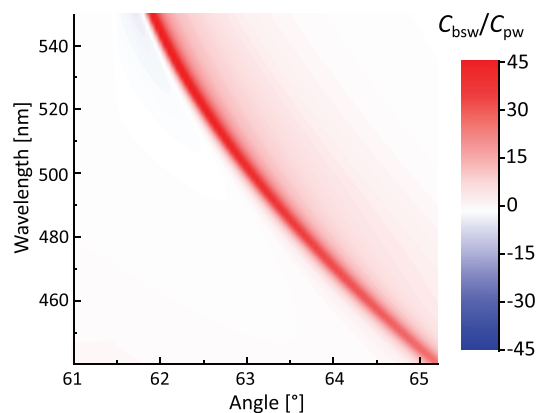


Figure 3. Predicted optical chirality enhancement $C_{\text{bsw}}/C_{\text{pw}}$ for the proposed 1DPC, following the numerical calculation procedure in ref. [3], as a function of the wavelength and of the angle of incidence.

The excitation of the surface wave manifests itself as a dip in the reflectivity spectrum, due to the non-negligible material absorption. Although the slight residual misalignment confirms that there is still some room for improvement, the exceptional parallelism between the two bands and their good partial overlap already provide the possibility to, for example, generate BSWs characterized by strong and broadband “superchiral” electromagnetic fields. This is numerically confirmed by the plot in **Figure 3**, where the predicted optical chirality enhancement (compared to plane-wave illumination) that can be generated at the surface is calculated following the procedure already established in ref. [3] and comparably large enhancement factors are indeed predicted.

2.2. Multilayer Fabrication

The BSW multilayer platform was fabricated by stacking a series of compact high refractive index (n_H) layers (Ta_2O_5) and low refractive index (n_L) layers (SiO_2) on a BK7 standard coverslip substrate with a stack distribution that optimizes the performance when working in contact with aqueous-based solutions.

The Ta_2O_5 and SiO_2 thin film layers (Figure 1a) were sequentially deposited by reactive magnetron sputtering using, respectively, tantalum and silicon targets (75 mm diameter) and a source operated with a pulsed DC power supply (AE Pinnacle Plus +, frequency 120 KHz, reverse time 2.5 μs). The process gas consisted of a mixture of Ar (40 sccm) and O_2 (4 sccm) at a pressure of 5.0×10^{-3} mbar. The multilayers were prepared at 150 $^\circ\text{C}$ and the magnetron target-substrate distance was approximately 10 cm. The sample holder was continuously rotated during the deposition process to achieve a homogeneous thickness over the entire exposed surface area. The base pressure of the deposition apparatus was 5×10^{-8} mbar. Figure 1b shows an experimental SEM cross-section image of one of the truncated 1DPC manufactured on a polished silicon wafer. The image shows compact deposited material and sharp interfaces between adjacent layers. SEM images were taken with a Hitachi S4800 field emission

electron microscope operated at 2.0 kV in backscattered mode. Brightness contrast between layers is due to the different atomic weights of the Ta₂O₅ and SiO₂ layers. The calibration of the growth parameters was performed with a trial-and-error procedure against the simulated normal-incidence reflectance spectra of the nominal design, while controlling the deposited thickness with a quartz microbalance.

2.3. Fluidic Chamber

Characterization of the optical performance of the sensing platform was done with water flowing over the surface of the photonic crystals thanks to a two-layer microfluidic circuit, closed at the bottom by the photonic crystal. The intermediate layer consists of a polymeric double-side tape (ARclad 8314-10, Adhesives Research, Inc., 193 μm thickness) with the fluidic chamber cut in it. The top layer is a fused silica slide that contains the housing to plug the fluidic tubes. These two layers are shaped using femtosecond laser (FemtoREGEN, High Q Laser GmbH, 1040 nm wavelength) micromachining.^[38] In the case of the fluidic chamber, its profile is ablated into the polymeric tape. The fundamental laser beam (100 kHz repetition rate) is steered on top of a computer-controlled translational stage using a series of high-quality high-reflectance mirrors. The polymeric tape is mounted on a horizontal plate fixed on the translation stages and the laser beam approaches vertically from the top. The focusing lens (20× microscope objective, 0.35 numerical aperture, NA) is mounted onto an independent holder with micromanipulators for high precision displacement and tilt control. The final product is an elongated chamber (8 mm × 4 mm) with short inlet and outlet channels. The top layer consists of a fused silica substrate (20 mm × 20 mm × 1 mm), with 3D clepsydra reservoirs inscribed into it through femtosecond laser micromachining followed by chemical etching.^[39] For the irradiation, we used the second harmonic of the same laser, at 1 MHz repetition rate focused by a 63× (0.75 NA) microscope objective, a subsequent etching process in a 20% HF aqueous solution reveals the 3D reservoirs. Their clepsydra profile allows for the easy plug and unplug of microfluidic peek tubes, avoiding liquid leakages during the filling process and the entire measurement. The three layers are fabricated separately and finally aligned and bonded together in order to obtain the closed fluidic device. A representative picture of the final system is shown in Figure S2, Supporting Information.

2.4. Experimental Characterization

We used an optical setup in the Kretschmann configuration for the excitation of BSWs. Polychromatic light from a LED source is coupled to a multimode optical fiber (core diameter: 50 μm, NA: 0.22) and collimated using a lens. Then, a polarizer allows setting the linear polarization of the light beam, varying between TE and TM conditions. Finally, the polychromatic light beam is coupled to a LASF9 coupling prism and to the 1DPC microfluidic chip that is optically matched on its base using immersion oil (refractive index $n = 1.7$). The intensity of the reflected light

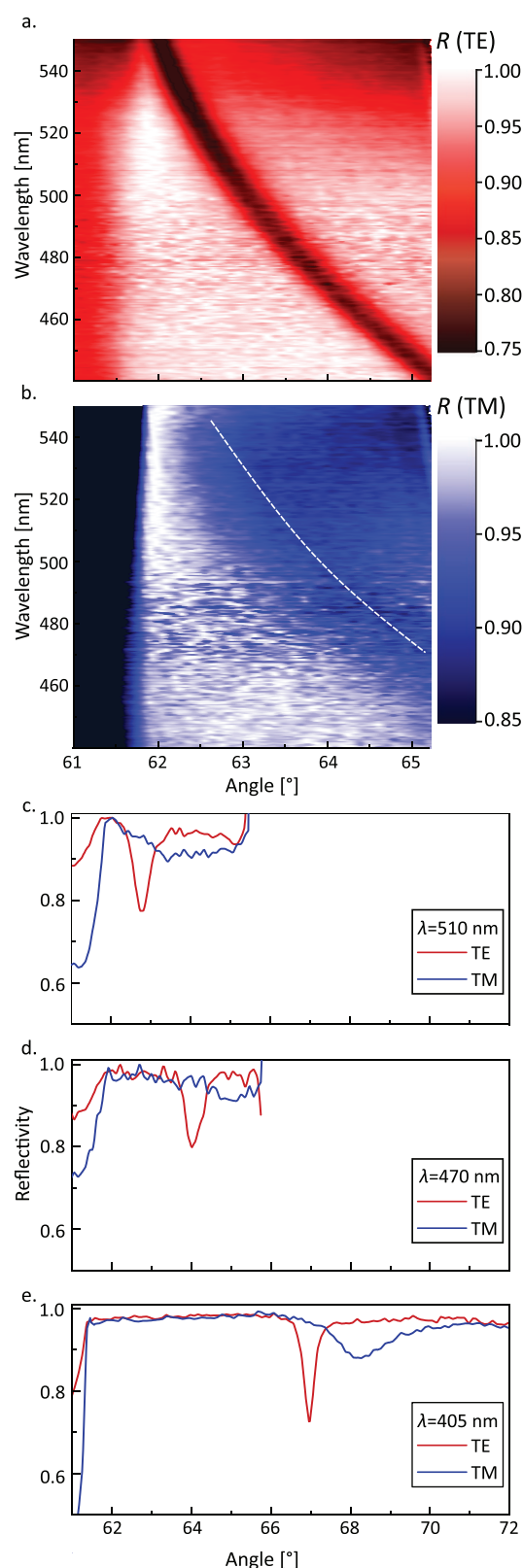


Figure 4. Experimental reflectivity (R) maps for a) TE illumination and b) TM illumination when the surface is immersed in water. The dispersive TE and TM modes are visible as dips in the reflectivity maps. Experimental angular plot for a wavelength λ equal to c) 510, d) 470, and e) 405 nm.

beam is collected by a 200 μm -core diameter multimode fiber, which is connected to a spectrometer (OceanOptics HR4000). The angle of incidence of the light beam onto the 1DPC and the collection angle of the detection fiber are controlled using rotational stages in a $\theta-2\theta$ configuration to measure the specular reflectivity spectra. The fluidic chamber is filled using micro-fluidic tubes (external diameter $\approx 360 \mu\text{m}$) with an aqueous solution. The sample-detector rotation and the data collection from the sensor are controlled using home-developed LabView software. With the LED light source, it is possible to investigate a broadband spectral range that, however, does not reach below 430 nm wavelength. For completeness, we also use a similar experimental setup to investigate one further wavelength in the blue region. For this additional measurement, the LED light source is substituted by a diode laser emitting at 405 nm wavelength, while the spectrometer is replaced by a Si switchable-gain detector. A sketch of the setup is depicted in Figure S3, Supporting Information. In order to assess the accuracy of the setup and validate the numerical analysis, we performed a preliminary characterization of the platform with aqueous glucose solutions at a wavelength of 405 nm as a function of the glucose concentration, as customarily done for standard refractometric sensing applications. We experimentally obtained an angular shift of the TE mode of about 13.4 $^\circ$ /RIU (refractive index unit) in excellent accordance with numerical predictions (Figure S4, Supporting Information).

3. Results and Discussion

For the experimental demonstration of the alignment and superposition of the TE and TM dispersion relations, reflectance measurements are performed on the 1DPC with the fluidic chamber filled with water.

The investigated wavelength range of the reflectivity maps (Figure 4a,b) spans from 430 to 600 nm, while the angular one extends from 60 $^\circ$, just before the total internal reflection onset, to about 68 $^\circ$. Representative angular plots extracted from the maps are shown in panels c and d. The additional spectrum measured at 405 nm (panel e) is acquired over a wider angular range extending from 60 $^\circ$ to 75 $^\circ$, to investigate the BSW modes at shorter wavelengths and higher excitation angles. All incidence angles refer to the direction of the excitation wavevector inside the substrate with respect to the surface normal. For better visualization of the features in the reflectivity maps, the signal coming from the photonic crystal is normalized to the reflectance of water collected from the coupling prism (without the 1DPC). The behavior of the surface modes is reproduced with high fidelity by the simulations: upon increasing the wavelength, the excitation angle of the modes decreases, approaching the onset of the total internal reflection. Moreover, it can be observed that, while the TE mode is narrow and sharp, the TM is broader and weaker, as expected. It can be noticed how, as the wavelength decreases, the TM mode becomes sharper and more clearly recognizable, allowing us to experimentally confirm the mode superposition predicted by numerical simulations.

As a final remark, it should be noted that the residual misalignment between the TE and TM modes must be attributed to a slight uncertainty, during the initial design, about the exact

dielectric functions of the deposited materials. To confirm that such a misalignment is indeed not an intrinsic limitation of the simplified 1DPC design introduced in this work, we report in Figure S5, Supporting Information, the results of a further numerical optimization, obtained by changing the layer thicknesses by less than 15% and employing the same dielectric functions as in Figure 2. The optimization results demonstrate that an excellent mode superposition over a broad spectral range can still be obtained also with this novel design. Moreover, to confirm that the experimental misalignment observed in this work does not compromise the polarization performance of the photonic platform, we simulated the optical chirality enhancement of such an optimized design as shown in Figure S6, Supporting Information, and find that it is predicted to be larger by less than a factor of 2 compared to the results of Figure 3. Finally, in Figure S7, Supporting Information, we compare the TE and TM reflectivity from three nominally identical samples, featuring a slightly different design compared to the main manuscript, in order to assess the robustness of the deposition procedure.

4. Conclusions

In conclusion, we realized a 1DPC characterized by a simple design and implemented it with well-established fabrication processes. The optical characterization of the platform was performed by acquiring angle-resolved reflectance spectra, which demonstrate that the TE and TM surface modes display overlapping dispersion relations over a broadband spectral range. This feature enables polarization control of the surface modes and paves the way for the implementation of polarization-resolved surface-enhanced techniques. In particular, our platform will be employed in CD measurements to enhance our capability to detect chiral molecules and perform polarization-dependent optical spectroscopy.

Supporting Information

Supporting Information is available from the Wiley Online Library or from the author.

Acknowledgements

P.B. acknowledges Matteo Tommasini and Maria Elisabetta Brenna for insightful discussions on chiroptical spectroscopy. F.Y. acknowledges MCIN for Salvador de Madariaga grant PRX19/00485 and project PID2019-110430GB-C21 funded by MCIN/AEI/10.13039/501100011033 and ERDF. This work was partially supported by the Grant PON ARS01_00906 "TITAN – Nanotecnologie per l'immunoterapia dei tumori", funded by FESR in the framework of PON "Ricerca e Innovazione" 2014 -2020 – Azione II – OS 1.b).

Open Access Funding provided by Politecnico di Milano within the CRUI-CARE Agreement.

Conflict of Interest

The authors declare no conflict of interest.

Data Availability Statement

The data that support the findings of this study are available from the corresponding author upon reasonable request.

Keywords

circular dichroism spectroscopy, linear dichroism spectroscopy, photonic crystals, surface-enhanced spectroscopy, surface waves

Received: March 31, 2022

Revised: June 24, 2022

Published online: August 19, 2022

- [1] J. D. Joannopoulos, S. G. Johnson, J. N. Winn, R. D. Meade, *Photonic crystals*, Princeton University Press, Princeton, New Jersey, USA **2008**.
- [2] A. Sinibaldi, N. Danz, E. Descrovi, P. Munzert, U. Schultz, F. Sonntag, L. Dominici, F. Michelotti, *Sens. Actuators, B* **2012**, *174*, 292.
- [3] G. Pellegrini, M. Finazzi, M. Celebrano, L. Duò, P. Biagioni, *Phys. Rev. B* **2017**, *95*, 241402.
- [4] G. Pellegrini, M. Finazzi, M. Celebrano, L. Duò, P. Biagioni, *Chirality* **2018**, *30*, 883.
- [5] F. Giorgis, E. Descrovi, C. Summonte, L. Dominici, F. Michelotti, *Opt. Express* **2010**, *18*, 8087.
- [6] G. M. Smolik, N. Deschermes, H. P. Herzig, *ACS Photonics* **2018**, *5*, 1164.
- [7] L. Fornasari, F. Floris, M. Patrini, G. Canazza, G. Guizzetti, D. Comoretto, F. Marabelli, *Appl. Phys. Lett.* **2014**, *105*, 053303.
- [8] B. Nordén, *Appl. Spectrosc. Rev.* **1978**, *14*, 157.
- [9] B. Nordén, G. Lindblom, I. Jonáš, *J. Phys. Chem.* **1977**, *81*, 2086.
- [10] R. Murrington, T. R. Dafforn, D. J. Halsall, A. Rodger, *Biophys. J.* **2004**, *84*, 2002.
- [11] P. Ferenci, *Aliment. Pharmacol. Ther.* **2004**, *19*, 157.
- [12] R. W. Smithells, C. G. H. Newman, *J. Med. Genet.* **1992**, *29*, 716.
- [13] Y. Tang, A. E. Cohen, *Phys. Rev. Lett.* **2020**, *104*, 163901.
- [14] Y. Tang, A. E. Cohen, *Science* **2011**, *332*, 333.
- [15] E. Hendry, T. Carpy, J. Johnston, N. Popland, R. V. Mikhaylovskiy, A. J. Laphorn, S. M. Kelly, L. D. Barron, N. Gadegaard, M. Kadodwala, *Nat. Nanotechnol.* **2010**, *5*, 783.
- [16] M. Schäferling, X. Yin, H. Giessen, *Opt. Express* **2012**, *20*, 26326.
- [17] M. Schäferling, X. Yin, N. Engheta, H. Giessen, *ACS Photonics* **2014**, *1*, 530.
- [18] M. L. Nesterov, X. Yin, M. Schäferling, M. Giessen, T. Weiss, *ACS Photonics* **2016**, *3*, 578.
- [19] N. A. Abdulrahman, Z. Fan, T. Tonooka, S. M. Kelly, N. Gadegaard, E. Hendry, A. O. Govorov, M. Kadodwala, *Nano Lett.* **2012**, *12*, 977.
- [20] M. Schäferling, N. Engheta, H. Giessen, T. Weiss, *ACS Photonics* **2016**, *3*, 1076.
- [21] A. O. Govorov, Z. Fan, P. Hernandez, J. M. Slocik, R. R. Naik, *Nano Lett.* **2010**, *10*, 1374.
- [22] A. O. Govorov, Z. Fan, *ChemPhysChem* **2012**, *13*, 2551.
- [23] E. Hendry, R. V. Mikhaylovskiy, L. D. Barron, M. Kadodwala, T. J. Davis, *Nano Lett.* **2012**, *12*, 3640.
- [24] M. Schäferling, D. Dregely, M. Hentschel, H. Giessen, *Phys. Rev. X* **2012**, *2*, 031010.
- [25] F. Lu, Y. Tian, M. Liu, D. Su, H. Zhang, A. O. Govorov, O. Gang, *Nano Lett.* **2013**, *13*, 3145.
- [26] Z. Wang, Y. Wang, G. Adamo, B. H. Teh, Q. Y. S. Wu, J. Teng, H. Sun, *Adv. Opt. Mater.* **2016**, *4*, 883.
- [27] Y. Liu, R. Wang, X. Zhang, *Opt. Express* **2014**, *22*, 4357.
- [28] V. K. Valev, J. J. Baumberg, B. De Clercq, N. Braz, X. Zheng, E. J. Osley, S. Vandendriessche, M. Hojeij, C. Blejean, J. Mertens, C. G. Biris, V. Volskiy, M. Ameloot, Y. Ekinci, G. A. E. Vandenbosch, P. A. Warburton, V. V. Moschchalkov, N. C. Panoiu, T. Verbiest, *Adv. Mater.* **2014**, *26*, 4074.
- [29] J. T. Collins, K. Ch, D. C. Hooper, C. Sibia, M. Centini, V. K. Valev, *Adv. Opt. Mater.* **2017**, *5*, 1700182.
- [30] M. Finazzi, P. Biagioni, M. Celebrano, L. Duò, *Phys. Rev. B* **2015**, *91*, 195427.
- [31] F. Mattioli, G. Mazzeo, G. Longhi, S. Abbate, G. Pellegrini, E. Mogni, M. Celebrano, M. Finazzi, L. Duò, C. G. Zanchi, M. Tommasini, M. Pea, S. Cibella, R. Polito, F. Sciortino, L. Baldassarre, A. Nucara, M. Ortolani, P. Biagioni, *ACS Photonics* **2020**, *7*, 2676.
- [32] J. E. Vázquez-Lozano, A. Martínez, *Laser Photonics Rev.* **2020**, *14*, 1900422.
- [33] J. García-Guirado, M. Svedendahl, J. Puigdollers, R. Quidant, *Nano Lett.* **2020**, *20*, 585.
- [34] M. L. Solomon, J. Hu, M. Lawrence, A. García-Etxarri, J. A. Dionne, *ACS Photonics* **2019**, *6*, 43.
- [35] M. Daimon, A. Masamura, *Appl. Opt.* **2007**, *46*, 3811.
- [36] L. Gao, F. Lemarchand, M. Lequime, *Opt. Express* **2012**, *20*, 15734.
- [37] V. Liu, S. Fan, *Comput. Phys. Commun.* **2012**, *183*, 2233.
- [38] R. Gattass, E. Mazur, *Nat. Photonics* **2008**, *2*, 219.
- [39] F. Sima, K. Sugioka, R. M. Vázquez, R. Osellame, L. Kelemenand, P. Ormos, *Nanophotonics* **2018**, *7*, 613.